# Tuning the exciton luminescence in an acoustically depleted two-dimensional electron gas

O. A. Korotchenkov* and A. Cantarero
*Materials Science Institute, University of Valencia, P.O. Box 22085, E-46071 Valencia, Spain*
(Received 15 September 2006; revised manuscript received 6 January 2007; published 23 February 2007)

Standing-wave piezoelectric fields can be used to vary spatially and temporally charge conditions in GaAs/AlGaAs quantum wells (QWs), offering a versatile tool to control the two-dimensional electron gas (2DEG) density in the well. A $LiNbO_3$ piezoelectric resonator imparts a MHz-frequency oscillating piezoelectric field with a controllable ratio of the in-plane and the vertical field components to a 2DEG placed in close proximity to the plate surface. This allows us to dynamically tune the charge state in the plane of the QW and to influence the photoluminescence spectra. It is found that spatially distributed regions of depleted and accumulated electron densities are formed in the QW plane due to the in-plane components of the piezoelectric field. The photoluminescence spectrum then varies both spatially and temporally, exhibiting an electron-hole plasma recombination at large electron densities and exciton and trion emissions at the extreme of small densities. Controlling the piezoelectric field component perpendicular to the QW layers allows us to achieve the spatially indirect exciton luminescence in double quantum well structures.

DOI: 10.1103/PhysRevB.75.085320 PACS number(s): 78.67.De, 78.20.Hp

Excitons and dense electron and hole gases in quantum wells (QWs) are among the key concepts in the optical and transport performance of quantum structures, providing a unique system for studies of collective states and many-body interaction effects. For example, in remotely *n*-doped QWs, where the excess two-dimensional electron gas (2DEG) density $n_{2D}$ can be continuously varied using a Schottky gate, the photoluminescence (PL) spectrum abruptly changes at a certain critical value of $n_{2D}$, which is typically a few $10^{10}$ $cm^{-2}$ excess electrons. Above the critical value, the Coulomb interaction between electrons and holes is mostly screened, which leads to a broad PL band indicative of the recombination of an electron plasma and a photoexcited valence-band hole. At densities below the critical value, the PL band evolves into two narrow peaks associated with the neutral $X$ (one electron bound to one hole) and negatively charged $X^-$ (two electrons bound to one hole) excitons.[1–4] The negatively charged excitons, or trions, are formed when excitons are present in an environment with excess electron densities. In order to control the excess charge density, two methods are commonly used, including the application of a bias voltage and the above barrier optical excitation with a high enough power.

Much effort has been undertaken to control the charge distribution by the piezoelectric field of acoustic waves.[5–7] The piezoelectric potential induced by the wave breaks up the initially homogeneous plasma into moving patterns of a reduced dimensionality, allowing us to manipulate the behavior of electrons and holes. For instance, dramatically prolonged times[5] and enhanced spin lifetimes[7] were obtained with the moving wires and dots of the electrons and holes separated by the piezoelectric potential of the surface acoustic wave. The accumulated electron density achieved in the piezoelectric field was reported to pump the stimulated emission in the QW.[8] A dynamic optical superlattice was obtained in a semiconductor microcavity modulated by stimulated acoustic phonons.[9]

Here, we report a process which offers dynamic control over the spatial distribution of electrons and holes in the plane of the QW and perpendicular to the plane, and allows for converting the plasma photoluminescence into the exciton and trion emissions. A bulk piezoelectric $LiNbO_3$ plate is used to impart an oscillating piezoelectric field with a controllable ratio of the field vector components to the QW charges placed in close proximity to the plate surface. Then it becomes possible to tune the charge environment for the photogenerated electron-hole pairs across the plane of the QW, which affects the luminescence properties.

The experiments were conducted using two samples grown by molecular-beam epitaxy. They consist of a $n^+$-type (001) GaAs substrate, a 100 nm GaAs Si doped ($10^{18}$ $cm^{-3}$) buffer layer, 20 periods of an undoped GaAs/$Al_xGa_{1-x}As$ QW structure, and a 50 nm $Al_{0.5}Ga_{0.5}As$ layer. A 30 nm GaAs cap layer covers the structure. The QW structure itself consists of a 6.1 nm QW separated by 50 nm $Al_{0.5}Ga_{0.5}As$ barriers (sample A) or an asymmetric double QW in sample B including a narrow well (width of 5.5 nm) as the top QW, which is closer to the surface, a barrier layer of $Al_{0.2}Ga_{0.8}As$ (thickness of 10 nm), and a wide well (width of 6.1 nm), separated from the next period by a 50 nm $Al_{0.5}Ga_{0.5}As$ barrier. In both samples, the distance between the upper QW and the surface was 80 nm. The linear dimensions of the samples were nearly the same. They were mounted on a cold finger in a helium cryostat and cooled down to a temperature of 6 K.

In experiments, MHz-frequency piezoelectric fields were achieved by mounting an optically transparent vibrating 128° *Y-X* cut $LiNbO_3$ piezoelectric plate ($3.8\times0.785\times13.8$ $mm^3$) onto the sample with the surface area of $8.5\times4$ $mm^2$. The sample was turned to the plate by its QW side, as shown in Fig. 1. The plate was electrically excited by a rf voltage $V$ applied to two electrodes (width of 1.5 mm), as discussed elsewhere.[10]

A 647.1 nm line of an $Ar^+$ laser was used to excite the sample through the $LiNbO_3$ plate in the normal-incidence geometry. The excitation energy is above the exciton ground states in the QWs in both the samples but lies below the band gap of the $Al_{0.5}Ga_{0.5}As$ barrier material, so that significant light absorption occurs only in between these barrier layers. The PL light was transmitted by the transparent $LiNbO_3$

 

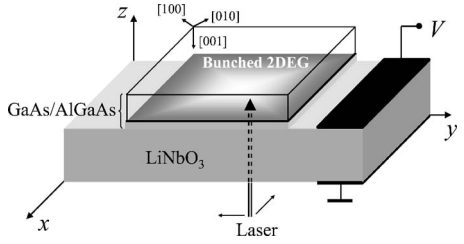


FIG. 1. Geometry of a hybrid system consisting of a 128° *Y-X* cut $LiNbO_3$ plate and a $GaAs/Al_xGa_{1-x}As$ QW structure. A Cartesian coordinate system $(x,y,z)$ is introduced such that the GaAs [100] and [010] crystal axes make angles 45° with the sample edges. The structure is placed down onto the piezoelectric plate by its 2DEG face. It is slightly pressed against the plate with a brass spring (not shown here). Interaction with the 2DEG is mediated via the piezoelectric field generated on the surface of the plate and penetrating into the QW structure.

plate and analyzed using a double monochromator with a spectral resolution of 0.05 meV. Detection was performed either, timeintegrating, with a charge coupled device or, time resolving, with a photomultiplier tube (Hamamatsu R928) followed by a boxcar averager (PAR model 162). In the latter case, the PL signal was averaged over the aperture of about 0.05 $\mu$s. By changing the aperture delay, the PL detection moment shifted along the time scale within the period of the standing-wave piezoelectric potential ($\approx$1.2 $\mu$s). 2D mapping measurements of the PL spectra were carried out by using a micromotion *x-y* stage. The laser beam was focused on the sample surface down to a diameter of $\approx$100 $\mu$m, penetrating a few micrometers deep inside the sample (absorption length $\approx$0.5 $\mu$m), well below the QW structure. The laser power was 10 mW or 125 $W/cm^2$ into the 100-$\mu$m-diam spot. This corresponds to the photogeneration rate of $1.2\times10^{19}$ $cm^{-2}$ $s^{-1}$ in the QWs assuming the surface reflectivity of 0.3 and the absorption coefficient of $2\times10^4$ $cm^{-1}$. Taking a free carrier lifetime of about 1 ns,[11] this amounts to a density of photoexcited electron-hole pairs $\approx10^{10}$ $cm^{-2}$.

The 2DEG is actuated by exciting the $LiNbO_3$ rectangular plate at a frequency coinciding with one of its resonant frequencies. In order to attain accompanying piezoelectric fields and mechanical stresses, a two-layer sandwich structure, including the $LiNbO_3$ and GaAs parallelepiped-shaped layers, was treated variationally. This was done by using a general computation scheme based on the study of Holland and Eer Nisse[12] and by extending it[13] to take into account boundary conditions at an interface between two materials that differ in elastic, piezoelectric, and dielectric properties. In the system assembly shown in Fig. 1, two boundary conditions are in order.

The first is the case where the $LiNbO_3$ and GaAs media are rigidly bounded together. This results in a continuity in displacement and stress across the interface. Using the case of a slippery condition where transverse slip of the bounded media may occur, a more accurate description of our hybrid system can be achieved. This requires the shear components of the stress to be zero at the interface. However, mechanical coupling of the two sliding media through the normal component of the stress ($T_{zz}$) can exist, depending on the force that presses the sample against the plate surface, which leaves ambiguity in the correct choice of boundary conditions.

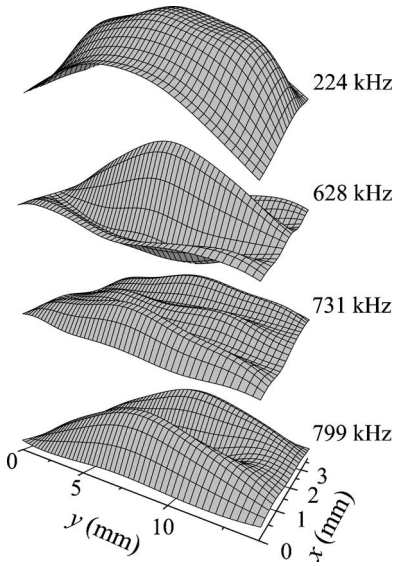


FIG. 2. Simulated normal stress profiles at $LiNbO_3$/GaAs interface at the selected resonant frequencies for the rigid contact conditions. The applied voltage is 10 V. The peak amplitudes of $T_{zz}$ are (in MPa) 10.3, 7.9, 3.6, and 4.5 from top to bottom. The components of the stress tensor rotated to GaAs crystallographic axes (cf. Fig. 1) are (in MPa) $T_{xx}$=1.2, $T_{xy}$=0.4, $T_{xz}$=0.8, $T_{yy}$=3.5, and $T_{yz}$=0.5 at the 731 kHz vibration frequency.

Representative profiles of $T_{zz}$, computed at the interface with the rigidly bounded media, are plotted in Fig. 2 at a number of structure resonances. Making a judicious choice of vibration mode to minimize the mechanical coupling through the normal stress, plate vibrations at about 740 kHz exhibiting the lowest $T_{zz}$ value were employed in this study. Here, we were able to experimentally resolve some effects on vibration frequency, which we believe provide a useful check on the interplay between the mechanical and electrical coupling of the two media. The use of varying mechanical and electrical conditions at the interface displayed a distinctive behavior of the resonance frequency that is expected in piezoelectrically coupled media.

Thus, a freely supported $LiNbO_3$ plate exhibits the resonance frequency of $\approx$740 kHz. The placement of a semiconductor on the plate surface always shifted the resonance to lower frequency. When we carried the sample on into the holder shown in Fig. 1, the shift was about 3.5 kHz. The use of a separate-medium structure with a vibrating plate freely supported above the sample appeared to cause this frequency shift to decrease (e.g., $\approx$3.2 kHz shift for $\approx$10 $\mu$m air gap between the $LiNbO_3$ and GaAs media). In contrast, after the sample was glued down onto the plate, a greater frequency shift was observed, as expected theoretically (e.g., 9 kHz shift for the 731 kHz vibration frequency in Fig. 2). Clearly, both the latter facts might have been expected given that, in our hybrid structure, the semiconductor sample and the driving $LiNbO_3$ plate are acoustically mismatched, offering the coupling of free carriers in the QWs to the plate through the

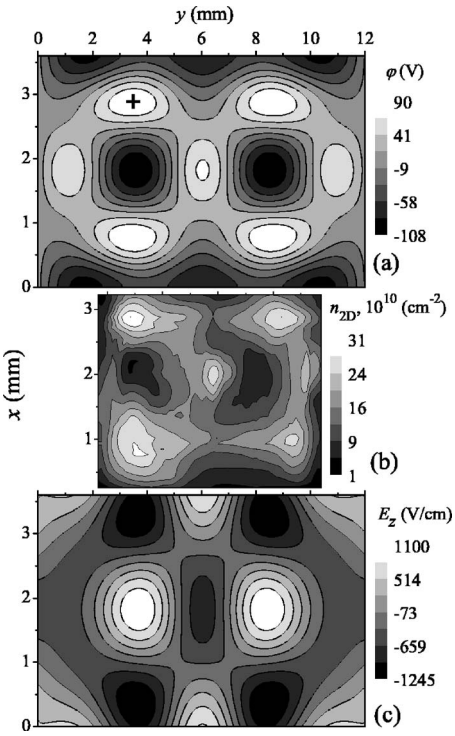


FIG. 3. Computed distributions of the (a) piezoelectric potential and (c) $E_z$ component of the field on the surface of the $LiNbO_3$ plate at its resonant vibration frequency of 740 kHz. The applied voltage is 10 V. (b) In-plane 2DEG density gated by the piezoelectric potential at $V=100$ V, as obtained from the PL line shape in sample A (see text). The symbol+ in panel (a) indicates the PL excitation and detection point for the spectra displayed in Figs. 4 and 5.

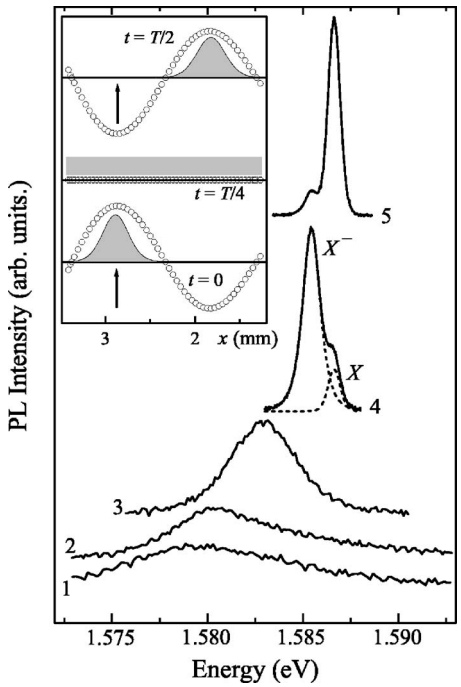


FIG. 4. Time-resolved PL spectra of sample A taken at times (1) $t=0$, (2) $T/8$, (3) $T/4$, (4) $3T/8$ and (5) $T/2$ with $T$ as the standing-wave period. The applied voltage is 100 V. The dashed lines illustrate the decomposition of spectrum 4 into $X$ and $X^-$ lines by Gaussian and Lorentzian functions, respectively. Inset: The piezoelectric potential distribution across the $x$ axis ($y=3.6$ mm) at times $t=0$ [cf. panel (a) in Fig. 3], $T/4$, and $T/2$ corresponding to spectra 1, 3, and 5, respectively. The shaded regions schematically illustrate the corresponding 2DEG density distributions. The arrow indicates the laser excitation point [symbol+ in Fig. 3(a)].

piezoelectric field extending beyond the plate and penetrating inside the sample. This produces an oscillating electric field in the QWs, which is reduced because of the dielectric constant of the sample $\varepsilon_s=12.5$, and the free electrons and holes will try to relax to this field.

In the present work, the amplitude of the piezoelectric field is specified in terms of the applied voltage amplitude $V$. The computed distributions of the potential and vertical ($E_z$) component of the field strength are shown in Figs. 3(a) and 3(c), respectively, exhibiting the spatial position of nodes and antinodes in the standing wave. Partly, in an attempt to check the consistency of these results, the computed $\varphi(x,y)$ distribution was compared to the experimental one taken with a sharp metal tip brought close to the plate surface. The measured distribution was observed to agree with the simulated result fairly well.

The time-integrated PL spectrum of sample A consists of a broadband with ≈4.5 meV full width a half maximum peaked at 1.583 eV (not shown here), originating from the recombination of an electron plasma and a photoexcited valence-band hole. The evolution of the PL band, taken in the detection point marked by the symbol + in Fig. 3(a), with shifting the detection moment along the wave period is shown in Fig. 4. Also shown in the inset is the schematics of the 2DEG distribution along the $x$ axis in the QW plane driven by the piezoelectric potential. When applying a positive potential at the detection point at time $t=0$, the electrostatics favor an increased electron density in the QW region nearby (shadow area in the lower inset of Fig. 4), as the QW electrons are driven to move closer to the detection point by the attractive positive potential. The PL concomitantly broadens to 10 meV in spectrum 1 and redshifts compared to that taken without the field, as expected for the emission from a region of a high-density 2DEG.[1–4] As the external potential is decreased, the PL band narrows and blueshifts, so that the spectrum taken at $\varphi=0$ (spectrum 3 in Fig. 4) closely resembles the time-integrated PL observed in the absence of the field. As the potential at the detection point is further decreased to negative values, the QW electrons are driven to move in-plane out of this point (upper inset in Fig. 4 for the maximum negative potential). Consequently, two narrow emission lines of the neutral ($X$) and negatively charged ($X^-$) excitons dominate the PL (spectra 4 and 5 in Fig. 4), as expected for emission from a region with a decreased 2DEG density. Also, since the 2DEG density in the excitation region is decreased when increasing the time delay from $T/4$ to $T/2$, the $X$ line grows at the expense of the $X^-$ line (spectrum 5 compared to spectrum 4 in Fig. 4).

Comparison can then be made to the spatial distribution of $n_{2D}$ also taken in sample A. This was obtained from the line shapes of the plasma and exciton recombinations. From the linewidth $\gamma$ of the 2DEG luminescence varying with $V$, the electron density is[14] $n_{2D}=\gamma m_e/\pi\hbar^2$, where $m_e=0.067m_0$

is the electron effective mass and $m_0$ is the free-electron mass. Estimated from the linewidth of spectra 1–3 in Fig. 4, the electron density varies from $3\times10^{11}$ (spectrum 1) to $1\times10^{11}$ cm$^{-2}$ (spectrum 3), the latter being close to the value obtained from Hall measurements at $V=0$.

Treating the system of $X$ and $X^-$ excitons as a two-level system in equilibrium with the energy separation of $E_b$ (equal to 1.2 meV from the separation of the $X$ and $X^-$ lines in spectra 4 and 5 of Fig. 4), the density of the 2DEG is[15]

$$n_{2D}=\frac{m_e kT}{\pi\hbar^2}\ln\left(1+\frac{I_{X^-}}{I_X}e^{E_b/kT}\right),$$

where $I_{X^-}/I_X$ is the peak area ratio for the $X$ and $X^-$ lines which depends on $V$ (cf. dashed lines in spectrum 4 of Fig. 4), $k$ is the Boltzmann constant, and $T$ is the temperature. The electron density is then found to be $6\times10^{10}$ and $1\times10^{10}$ cm$^{-2}$ for spectra 4 and 5 in Fig. 4, respectively.

Next, fixing time moment $t=0$, the PL distribution over the QW plane is imaged, giving rise to $n_{2D}(x,y)$ distribution shown in Fig. 3(b). Consistent with the above picture, bunching of charge in the 2DEG is clearly seen, which matches the distribution of the piezoelectric potential rather well. Indeed, in the regions of a positive $\varphi$ [white areas in Fig. 3(a)], puddles of electrons are formed [white regions in Fig. 3(b)]. Alternatively, decreased electron densities are observed in the areas of a negative $\varphi$ [black areas in Figs. 3(a) and 3(b)]. It is seen that the minimum value of $n_{2D}$ in Fig. 3(b) is about $1\times10^{10}$ cm$^{-2}$, which is of the order of the photoexcited density. Therefore, this technique is well suited for effective depletion of 2D electron gases.

It should be noted that the lifetime of the photoexcited electron-hole pairs due to their radiative recombination is much less than the acoustic wave period. Hence, at any time moment $t$ allowing the depleted electron gas at a given PL detection point, the luminescence of excitons can be comparable to their emission in static electric fields. Furthermore, since the employed acoustic frequency is much lower than the conductivity relaxation frequency,[16] the 2DEG follows the time-varying piezoelectric potential distribution. As a result, the spatially and temporally distributed depleted and accumulated charge regions are formed in the plane of the QW, allowing to tune the plasma-exciton recombination processes both spatially and temporally.

The double QW PL in sample B exhibits a broad PL band $I_w$ arising in the wide well accompanied by a subsidiary emission band $I_n$, ≈10 meV higher in energy, coming from the narrow well (spectrum 1 in Fig. 5). Since the 2DEG emission probes the hole density and because the ratio $I_n/I_w$ of the integrated PL intensities of the narrow and wide QWs is 0.14 in spectrum 1, it is therefore apparent that the majority of photoexcited holes relax into the wide QW.

The evolution of the PL in the piezoelectric field (spectra 2 and 3 in Fig. 5) can be interpreted by a schematic description of the band profiles and above-the-barrier photogenerated electrons and holes shown in insets (a) and (b) of Fig. 5. For highly positive potential $\varphi$ at $t=0$, both QWs are

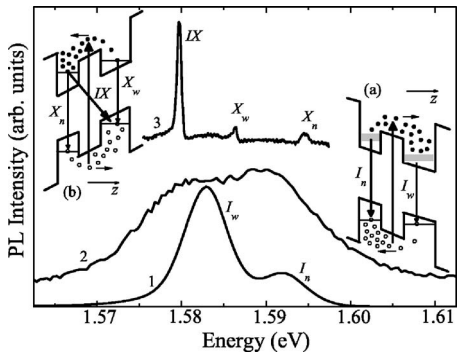


FIG. 5. (1) Time-integrated PL spectrum of sample B taken at $V=0$ and time-resolved spectra taken at $t=0$ (2) and $t=T/2$ (3) in the detection point indicated in Fig. 3. The applied voltage is 100 V. The insets schematically illustrate appropriate redistribution of photoexcited electrons (filled circles) and holes (open circles) between the narrow and wide QWs due to the $E_z$ component of the piezoelectric field. The vertical arrows show photoexcitation of electrons and holes (upward) and their recombination (downward). The shaded areas in (a) denote 2DEG.

populated with enhanced electron densities at the detection point; see inset (a). Accordingly, the linewidths of both the PL bands shown in spectrum 2 broaden by a factor of ≈2.4 compared to the ones in spectrum 1, as expected for emission from a region of increased $n_{2D}$. The photogenerated electrons and holes drift in the opposite directions under the $E_z$ component of the piezoelectric field (horizontal arrows in the inset). Cooling down through phonon-carrier and carrier-carrier scattering, they become trapped in the QWs, providing an increased hole population in the narrow QW. This increases the $I_n$ component of the PL, which is observed in spectrum 2 of Fig. 5.

Reversing $\varphi$ and $E_z$ at $t=T/2$ decreases the 2DEG density near the excitation point, so that the $Al_{0.5}Ga_{0.5}As$ interbarrier region is only filled with the photoexcited electrons and holes; see inset (b) of Fig. 5. Due to the drift of these carriers in the piezoelectric field (horizontal arrows in the inset), the majority of the electrons and holes are trapped in the ground states of the narrow and wide QWs, respectively. The resulting PL (spectrum 3 in Fig. 5) is dominated by a peak marked $IX$, which arises from the recombination of spatially indirect excitons with electrons and holes confined in the different QWs [transition $IX$ in inset (b) of Fig. 5]. Two weak features marked $X_w$ and $X_n$ in spectrum 3 originate from the recombination of direct excitons created in the wide and narrow QWs, respectively [transitions $X_w$ and $X_n$ in inset (b)]. As expected for the indirect exciton transitions, the peak energy of the $IX$ line has been observed to increase with moving the detection moment $t$ out from the $T/2$ value, which results from decreasing strength of the $E_z$ component of the piezoelectric field. In contrast, the $X_w$ and $X_n$ energies remained nearly unchanged, as expected for thin QWs.[17] It was also found that, upon increasing peak energy, the $IX$ line weakens in intensity, while the $X_w$ and $X_n$ lines strengthen and broaden seemingly at the expense of the $IX$ line, until eventually a double-band spectrum similar to spectrum 1 in Fig. 5 is observed at $t=T/4$ and $t=3T/4$.

In conclusion, the results presented here provide the evidence for varying the 2DEG density with a piezoelectric field of acoustic waves, opening the way for a controllable tuning of exciton luminescence in the presence of the electron gas. Although reported here for simple quantum well structures, it appears attractive to explore this technique to tune the population properties of various states in quantum systems and to achieve the population inversion in vertically coupled nanostructures.

O.A.K. thanks the Ministerio de Educación, Cultura y Deporte of Spain for financial support of this work.

*Permanent address: Department of Physics, National University of Kiev, Kiev 03680, Ukraine.

[1] K. Kheng, R. T. Cox, Y. Merle d'Aubigne, F. Bassani, K. Saminadayar, and S. Tatarenko, Phys. Rev. Lett. **71**, 1752 (1993).
[2] G. Finkelstein, H. Shtrikman, and I. Bar-Joseph, Phys. Rev. Lett. **74**, 976 (1995).
[3] A. J. Shields, M. Pepper, D. A. Ritchie, M. Y. Simmons, and G. A. C. Jones, Phys. Rev. B **51**, 18049 (1995).
[4] A. Ron, H. W. Yoon, M. D. Sturge, A. Manassen, E. Cohen, and L. N. Pfeiffer, Solid State Commun. **97**, 741 (1996).
[5] C. Rocke, S. Zimmermann, A. Wixforth, J. P. Kotthaus, G. Böhm, and G. Weimann, Phys. Rev. Lett. **78**, 4099 (1997).
[6] V. I. Talyanskii, J. M. Shilton, M. Pepper, C. G. Smith, C. J. B. Ford, E. H. Linfield, D. A. Ritchie, and G. A. C. Jones, Phys. Rev. B **56**, 15180 (1997).
[7] T. Sogawa, P. V. Santos, S. K. Zhang, S. Eshlaghi, A. D. Wieck, and K. H. Ploog, Phys. Rev. Lett. **87**, 276601 (2001).
[8] A. B. Nadtochii, O. A. Korotchenkov, and H. G. Grimmeiss, Phys. Rev. B **67**, 125301 (2003).
[9] M. M. de Lima, Jr., R. Hey, P. V. Santos, and A. Cantarero, Phys. Rev. Lett. **94**, 126805 (2005).
[10] A. M. Gorb, A. B. Nadtochii, and O. A. Korotchenkov, J. Phys.: Condens. Matter **15**, 7201 (2003).
[11] J. Feldmann, G. Peter, E. O. Göbel, P. Dawson, K. Moore, C. Foxon, and R. J. Elliott, Phys. Rev. Lett. **59**, 2337 (1987).
[12] R. Holland and E. P. Eer Nisse, IEEE Trans. Sonics Ultrason. **SU-15**, 119 (1968).
[13] O. I. Polovina, V. V. Kurylyuk, and O. A. Korotchenkov, cond-mat/0604337 (unpublished).
[14] R. Rapaport, G. Chen, D. Snoke, S. H. Simon, L. Pfeiffer, K. West, Y. Liu, and S. Denev, Phys. Rev. Lett. **92**, 117405 (2004).
[15] A. Manassen, E. Cohen, A. Ron, E. Linder, and L. N. Pfeiffer, Phys. Rev. B **54**, 10609 (1996).
[16] For the 2DEG, the conductivity relaxation frequency $\omega_c = \sigma k/\varepsilon_0(\varepsilon_s+\varepsilon_p)$, where $\sigma = en_{2D}\mu$ is the sheet conductivity, $e$ is the electron charge, $\mu$ is the electron mobility, $k$ is the acoustic wave number, and $\varepsilon_0$ and $\varepsilon_p$ are the dielectric constants of free space and of the piezoelectric plate, respectively [A. Wixforth, J. Scriba, M. Wassermeier, J. P. Kotthaus, G. Weimann, and W. Schlapp, Phys. Rev. B **40**, 7874 (1989), and references therein]. Taking appropriate values for the experiment, $\mu \approx 10^6$ cm$^2$/V s, $n_{2D} \approx 10^{11}$ cm$^{-2}$, $k \approx 10^3$ m$^{-1}$, and $\varepsilon_p \approx 50$, we find $\omega_c \approx 3 \times 10^{10}$ s$^{-1}$.
[17] D. A. B. Miller, D. S. Chemla, T. C. Damen, A. C. Gossard, W. Wiegmann, T. H. Wood, and C. A. Burrus, Phys. Rev. B **32**, 1043 (1985).